Published in final edited form as:
Mol Cancer Ther. 2012 October ; 11(10): 2183–2192. doi:10.1158/1535-7163.MCT-12-0552.

Active efflux of dasatinib from the brain limits efficacy against murine glioblastoma: broad implications for the clinical use of molecularly-targeted agents

Sagar Agarwal[1,2], **Rajendar K. Mittapalli**[1,2], **David M. Zellmer**[3], **Jose L. Gallardo**[3], **Randy Donelson**[3], **Charlie Seiler**[3], **Stacy A. Decker**[4], **Karen S. SantaCruz**[5], **Jenny L. Pokorny**[7], **Jann N. Sarkaria**[7], **William F. Elmquist**[1,2], and **John R. Ohlfest**[2,3,6,*]

[1]Department of Pharmaceutics, University of Minnesota, Minneapolis, MN, U.S.A.

[2]Brain Barriers Research Center, University of Minnesota, Minneapolis, MN, U.S.A.

[3]Department of Pediatrics, University of Minnesota, Minneapolis, MN, U.S.A.

[4]Department of Neuroscience, University of Minnesota, Minneapolis, MN, U.S.A.

[5]Department of Laboratory Medicine and Pathology, University of Minnesota, Minneapolis, MN, U.S.A.

[6]Department of Neurosurgery, University of Minnesota, Minneapolis, MN, U.S.A.

[7]Department of Radiation Oncology, Mayo Clinic, Rochester, MN, U.S.A.

Abstract

The importance of the blood-brain barrier in preventing effective pharmacotherapy of glioblastoma has been controversial. The controversy stems from the fact that vascular endothelial cell tight junctions are disrupted in the tumor, allowing some systemic drug delivery. P-glycoprotein (Pgp) and breast cancer resistance protein (BCRP) efflux drugs from brain capillary endothelial cells into the blood. We tested the hypothesis that although the tight junctions are “leaky” in the core of glioblastomas, active efflux limits drug delivery to tumor-infiltrated normal brain and consequently, treatment efficacy. Malignant gliomas were induced by oncogene transfer into wild-type (WT) mice or mice deficient for Pgp and BCRP (KO). Glioma-bearing mice were orally dosed with dasatinib, a kinase inhibitor and dual BCRP/PgP substrate that is being tested in clinical trials. KO mice treated with dasatinib survived over twice as long as WT mice. Microdissection of the tumor core, invasive rim, and normal brain revealed 2-3 fold enhancement in dasatinib brain concentrations in KO mice relative to WT. Analysis of signaling demonstrated that poor drug delivery correlated with the lack of inhibition of a dasatinib target, especially in normal brain. A majority of human glioma xenograft lines tested expressed BCRP or PgP and were sensitized to dasatinib by a dual BCRP/Pgp inhibitor, illustrating a second barrier to drug delivery intrinsic to the tumor itself. These data demonstrate that active efflux is a relevant obstacle to treating glioblastoma and provide a plausible mechanistic basis for the clinical failure of numerous drugs that are BCRP/Pgp substrates.

Keywords

Blood brain barrier; glioblastoma; kinase inhibitor; efflux; dasatinib

* † To whom correspondence should be addressed: John Ohlfest, Department of Pediatrics, University of Minnesota, 420 Delaware St. SE, MMC 366, Minneapolis, MN 55455. ohlfe001@umn.edu. .

The authors have no conflicts of interest to disclose.

Introduction

Glioblastoma multiforme (GBM) is a devastating primary brain tumor that claims more than 12,000 lives each year in the United States (1). Despite aggressive treatment, nearly all malignant gliomas recur (2), eventually leading to patient death. The median overall survival of patients with GBM is 16-19 months (3); survival after tumor recurrence is a dismal 5-7 months (4). Small molecule molecularly-targeted agents that target signaling pathways critical for tumor cell growth have been extensively evaluated for therapy in GBM (5). Unfortunately, none of these have resulted in any significant clinical benefit despite success in numerous preclinical models (6).

A critical challenge in treating most neurological diseases is delivery of drugs into the CNS (7). The blood-brain barrier (BBB) separates the brain from peripheral circulation and thus protects it from harmful toxins and chemicals (8). This physical barrier is largely attributable to the tight junctions between brain capillary endothelial cells that limit paracellular diffusion. Drug transporter proteins, such as the ATP-binding cassette transporters P-glycoprotein (Pgp, encoded by *ABCB1*) and the breast cancer resistance protein (BCRP, encoded by *ABCG2*), constitute a major component of this barrier and restrict drug penetration into the brain by effluxing them back into the blood (9). These transporters significantly limit the distribution of a number of drugs to the brain, including multiple anti-cancer agents currently used in clinic (10-17). Previous studies have shown that several molecularly-targeted tyrosine kinase inhibitors (TKI) are dual substrates for Pgp and BCRP, and as a result, have poor brain penetration (10-12). Simultaneous inhibition of both transporters demonstrated dramatic increases in brain penetration of these drugs, suggesting that it is necessary to inhibit both proteins to significantly improve the brain penetration of dual substrates (10-12).

The relevance of the BBB in treating brain tumors has been controversial. Imaging studies have long been known to reveal brain malignancies because the “leaky” tight junctions in the bulk tumor mass allow the imaging contrast agent to selectively accumulate in the tumor core. This clinical observation, along with recent studies that demonstrate robust TKI delivery into the core tumor mass (18, 19), have suggested that treatment failure with TKIs is not due to inadequate drug delivery. According to this hypothesis, the BBB is compromised by residual damage from radiotherapy, and/or by the tumor itself such that the functional integrity of the BBB is lost and drug delivery is not the basis for treatment failure (18, 19).

There is also evidence to support the counter hypothesis: that the BBB is not uniformly leaky, and drug delivery is a critical obstacle to treating GBM. Levin et al. experimentally demonstrated that BBB disruption in brain tumors is not uniform within the tumor or surrounding brain (20, 21). Glioma cells have the ability to invade normal brain tissue several centimeters away from the tumor, escaping surgical resection (22, 23). While the BBB might be disrupted at or near the tumor core, it remains intact in areas away from the core and consequently restricts delivery of anti-cancer drugs in these regions (24). This suggests that limited drug delivery to the invasive tumor cells may be a significant contributor to therapy resistance in many GBM patients. This kind of drug delivery failure is often not detected in preclinical models that are used to justify clinical trials. Some preclinical models used are not established in the brain (e.g., flank model), or assessments of anti-tumor efficacy involves mice bearing well-circumscribed brain tumors derived from implanted cell lines that exhibit a leaky BBB amid no appreciable infiltration. The latter well-circumscribed phenotype is the growth pattern of the majority of standard implanted models that are typically used for preclinical validation in the process of drug development

(25). If inadequate drug delivery is a plausible mechanism for the failure of TKIs in the clinic, then it is not surprising that clinical trials derived from these inadequate preclinical models have culminated in a series of disappointing failures.

Based on this premise, we hypothesize that restricted delivery of molecularly-targeted agents to the brain can significantly limit efficacy. We have used dasatinib as a model agent because we have shown that its brain penetration is limited by Pgp- and BCRP-mediated active efflux at the BBB (12) and it is currently being testing in clinical trials for GBM. Since active efflux limits the brain penetration of many drugs used to treat glioma, dasatinib is considered a reasonable surrogate to address the overarching question of how efflux at the BBB limits treatment efficacy. Using a highly infiltrative model of glioma, we demonstrate that increased delivery of dasatinib to the brain of mice deficient in Pgp and BCRP significantly enhances its efficacy. Our data suggest that inadequate drug delivery is a perfectly plausible, yet often discounted mechanism to explain the clinical failure of TKIs and warrants clinical investigation into using dual BCRP/Pgp pharmacologic inhibitors to improve drug delivery to GBM.

Material and Methods

Chemicals

Dasatinib (Figure 1) was purchased from LC Labs (Woburn MA). Texas Red Dextran 3000 MW (TRD) was purchased from Molecular Probes; Invitrogen (Eugene, Oregon, USA). Elacridar (GF120918) was obtained from Toronto Research Chemicals (Ontario, Canada).

Animal Care

All procedures were carried out in accordance with the guidelines set by the Principles of Laboratory Animal Care (National Institutes of Health) and were approved by The Institutional Animal Care and Use Committee of the University of Minnesota. FVB wild-type (WT) and *Mdr1a/b*$^{(-/-)}$*Bcrp1*$^{(-/-)}$ mice, hereafter referred to as knockout (KO) mice, were from Taconic Farms, Inc. (Germantown, NY).

Spontaneous Glioma Model

We used an oncogene induced *de novo* model of malignant glioma previously described by Wiesner et al. (26). Plasmid vectors coding for mouse platelet derived growth factor beta (mPDGFβ), enhanced green fluorescent protein (eGFP) and a short hairpin RNA against p53 (p53shRNA), and flanked by transposon IR/DR's, were mixed with a transfection agent, in vivo-jetPEI (PEI) (Polyplustransfection Inc., NewYork, NY), and a sleeping beauty (SB) transposase vector containing the luciferase reporter, in the ratio 2:2:1 (PDGF:p53:SB, respectively). Neonatal mice were secured in a cooled, "neonatal rat" stereotaxic frame (Stoelting, Wood Dale, IL) maintained at 4-8 °C and DNA-PEI complexes were injected into the right lateral ventricle (1 μg total DNA in 2 μL) using a 10 μL Hamilton syringe fitted with a 30-gauge hypodermic needle (Hamilton Company, Reno, NV). Mice were allowed to recover on a heated pad before moving them back to their cages. Tumors spontaneously arose after three-to-eight weeks as detected by bioluminescent imaging (26) (Figure 2). Animals were imaged regularly and were in enrolled in experiments when a measurable tumor was documented, as defined by a minimum signal of 2×10^5 photons/sec/cm^2/Sr.

Regional Breakdown of the Blood-Brain Barrier

Tumor-bearing WT mice were anaesthetized using ketamine (100 mg/kg) and xylazine (10 mg/kg). The animals were injected with TRD (1.5 mg/animal body weight) via the tail vein. TRD was allowed to circulate for 10 minutes, after which the animal was perfused by a brief

cardiac washout for 30 s. Following perfusion, the brain tissue was removed and flash frozen in isopentane (−60°C). Care was taken to remove brain rapidly in less than 60 s in order to minimize post mortem diffusion of the compound. Brains were then sectioned (20 μm) using a cryostat (Leica Cryotome®) at −20 °C. Brain sections were mounted on glass slides and air dried. After tissue preparation, fluorescent images were obtained using Leica inverted fluorescent microscopy (Model DMI6000B). The fluorescent image analysis was performed using Image J. To convert the fluorescent intensity to concentration, a standard reference curve was generated in brain homogenate as previously described (27).

Plasma and Brain Distribution of Dasatinib after oral dosing in FVB WT and KO mice

WT and KO mice (n = 28 per group) were administered 15 mg/kg dasatinib via oral gavage. Animals were sacrificed at pre-determined time points post dose (n = 4 at each time point). Blood was collected by cardiac puncture and plasma was harvested. Whole brain was immediately removed from the skull, rinsed with cold saline and flash frozen in liquid nitrogen. Plasma and brain specimens were stored at −80°C until analysis by LC-MS/MS for determination of dasatinib concentrations. Pharmacokinetic parameters from the concentration-time data in plasma and brain were obtained by non-compartmental analysis (NCA) performed using Phoenix WinNonlin 6.1 (Mountain View, CA). The area under the concentration-time profiles for plasma (AUCplasma) and brain (AUCbrain) was calculated using the linear trapezoidal method. The sparse sampling module in WinNonlin was used to estimate the standard error around the mean of the AUCs.

Brain Concentrations of Dasatinib

Tumor-bearing WT and KO mice were administered 15 mg/kg dasatinib via oral gavage (n = 5 - 10 per group). Animals were sacrificed 90 minutes post dose and the whole brain was harvested. With the aid of GFP visualization goggles (Biological Laboratory Equipment, Budapest, Hungary), the brain was immediately dissected into core, rim (brain around tumor) and normal brain. Since the tumor expresses GFP, the region of concentrated green fluorescence was deemed as the tumor core, the tissue surrounding the tumor was called as tumor rim and normal brain tissue was collected from the left (contralateral) hemisphere. Tissue specimens were flash frozen in liquid nitrogen and stored at −80°C until further analysis.

Dasatinib concentrations in the tissue specimens were determined by a rapid and sensitive LC-MS/MS method. Frozen samples were thawed at ambient temperature. Brain samples were homogenized using 3 volumes of 5 % bovine serum albumin in phosphate-buffered saline and a 100-μL aliquot of brain homogenate or plasma was used for analysis. Samples were spiked with 10 ng of gefitinib as internal standard and alkalinized by addition of 200 μL of a pH 11 buffer (1 mM sodium hydroxide, 0.5 mM sodium bicarbonate). The samples were then extracted by liquid-liquid extraction using ice-cold ethyl acetate. A 5-μL volume of sample was injected in the HPLC system. Chromatographic analysis was performed using an Agilent Model 1200 separation system and an Agilent Eclipse XDB-C18 RRHT threaded column (Santa Clara, CA, USA). The mobile phase was composed of acetonitrile: 20mM ammonium formate (containing 0.1% formic acid, pH 4) (32:68 v/v). The column effluent was monitored using a Thermo Finnigan^{TM} TSQ® Quantum 1.5 detector (San Jose, CA, USA) to allow the $[MH]^+$ ion of dasatinib at *m/z* 488 and that of internal standard at *m/z* 446.9 to pass into the collision cell. The product ions for dasatinib (*m/z* 401) and the internal standard gefitinib (*m/z* 128.1) were monitored through the third quadrupole. The lower limit of detection of the assay was at least 2.5 ng/ml with a corresponding CV of ~ 10%.

Regional Efficacy of Dasatinib by Target Inhibition using Western Blot

A separate group of WT and KO mice (n = 4 per group) were treated with vehicle or dasatinib (15 mg/kg) for three days. Mice were sacrificed and the whole brain was dissected into core, rim (brain around tumor) and normal brain using the GFP visualization goggles as described above. Western blotting was conducted in the tissue specimens for determination of expression levels of AKT, phospho-AKT, SRC, phospho-SRC and beta-actin as a control for protein loading. Tissue specimens were lysed in radioimmunoprecipitation assay buffer containing protease and phosphatase inhibitors. Protein concentration was determined using the bicinchoninic acid assay and 40 μg were loaded per lane on a 4% to 12% SDS-PAGE gel, and run at 170 volts for 1 hour. Gels were transferred to a nitrocellulose membrane and blots were then incubated with the primary antibodies to pSRC, SRC, pAKT, AKT and actin (1:1000, Cell Signaling, MA) overnight at 4 °C. Membranes were washed and incubated with horseradish peroxidase (HRP)-conjugated secondary antibody (1:1000, Cell Signaling, MA) for 1 hour. Proteins were detected using Amersham ECL™ Advance Western Blotting Detection Kit (GE Life Sciences, NJ).

Efficacy of Dasatinib in the Spontaneous Glioma Model

Oncogene-injected mice were imaged regularly to detect tumor formation and were enrolled in a treatment arm within a day of reaching the tumor signal threshold (minimum of 2×10^5 photons/sec/cm^2/Sr). Mice were randomly assigned to one of four groups (n = 5 - 8 per group); (i) WT mice treated with 15 mg/kg dasatinib, (ii) WT mice treated with vehicle, (iii) KO mice treated with dasatinib and (iv) KO mice treated with vehicle. All mice received either dasatinib or vehicle by oral gavage every 12 hours for seven days and survival was monitored post treatment initiation with the experimental endpoint being death or moribund status of the mice.

Efficacy of Dasatinib and Transporter Expression in Human GBM Cell Lines

The short-term explant cell lines used in this study were derived from primary human GBM specimens and have been maintained by serial xenotransplantation in mice as previously described in detail (28). The xenograft lines were established and exclusively maintained in the Sarkaria laboratory. Therefore, no authentication was performed. For drug sensitivity assays, 5,000 cells per well were cultured in the presence of 0, 0.3, 1, and 10 μM of dasatinib with or without 5 μM of GF120918, a dual BCRP/PgP inhibitor. Seventy-two hours later, cell viability was measured using an MTS assay as previously described (29). The cell-survival data in the GBM cell lines was analyzed using an inhibitory sigmoid E_{max} model. The IC_{50} values were estimated and compared between the control and GF120918 treated groups. For western blots, primary antibodies to beta-actin (1:1000, Cell Signalling, MA), ABCB1 (p-glycoprotein (c219), 1:100) and ABCG2 (BXP-21, 1:500), (Enzo Life sciences, NY) were used. HRP-conjugated anti-mouse (1:20,000, Pierce,) and anti-rabbit (1:5000, Cell Signaling, MA) secondary antibodies were used for detection.

Statistical Analyses

Animal survival was analyzed with Prism 4 software (Graph Pad Software, Inc.) using a log-rank test. For all other experiments statistical analyses were made with SigmaStat, version 3.1 (Systat Software, Inc.) using a two-tailed *t-test*.

Results

Regional Breakdown of the Vascular Endothelial Cell Tight Junctions

We utilized an oncogene-induced *de novo* model of murine GBM (26), with one modification, the replacement of the *NRAS* oncogene with *mPDGFβ*. The *firefly luciferase*,

eGFP and *p53shRNA* genes were delivered on separate vectors as before (Figure 2A). Tumors arose within 4-8 weeks of birth and progressed rapidly, killing animals within two weeks or less from the time of initial detection using bioluminescent imaging. Representative histological analysis of a tumor from a moribund animal is shown in Figure 2B. Hallmark features of GBM were apparent, including diffuse infiltration of tumor cells into the surrounding normal brain tissue (e.g., absence of clear tumor:brain boundary), necrosis, and microvascular proliferation. Importantly, similar to human patients, these tumors formed at different locations within the brain of each animal, introducing a source of spatial heterogeneity not modeled in transplanted models. In order to determine if this model had defects in the capillary endothelial cell tight junctions similar to human GBM, a 3kDa TRD probe was systemically administered and allowed to circulate for 10 minutes. TRD brain penetration was analyzed in microdissected tumor (based on GFP) and normal brain. Microscopic analysis revealed large tumors with a heterogeneous distribution of TRD within the center of the mass and less TRD accumulation in adjacent normal brain (Figure 3A). Quantitation of TRD demonstrated over a three-fold increase in TRD in the GFP^{bright} tissue harboring the tumor core relative to the adjacent normal brain (Figure 3B). This animal model therefore resembles a spatially heterogeneous breakdown of the tight junctions similar to human GBM.

Plasma and Brain Distribution of Dasatinib in Mice

We compared the plasma and brain distribution of dasatinib between WT and KO mice. Plasma concentrations of dasatinib after oral dosing in the KO mice were not significantly different than that in WT mice ($p > 0.05$, Figure 4A). The AUCplasma was 1.31 μg.hr/ml in the WT mice compared to 1.78 μg.hr/ml in the KO mice ($p > 0.05$, Supplementary Table 1). This indicates that P-gp and BCRP have minimal influence on the oral absorption or systemic clearance of dasatinib at the 15 mg/kg dose. Dasatinib brain concentrations were significantly enhanced in KO mice compared with those in the WT mice ($p < 0.05$; Figure. 4B). The AUCbrain was 0.160 μg.hr/ml in the WT mice and increased by approximately 10-fold to 1.63 μg.hr/ml in the KO mice ($p = 0.001$). The ratio of AUCbrain to AUCplasma in WT mice was ~ 0.12, indicating the restriction to brain penetration of dasatinib. This ratio increased by 7-fold to 0.93 in the KO mice (Supplementary Table 1). These results conclusively demonstrate that dasatinib brain distribution is dramatically enhanced when P-gp and BCRP are absent at the BBB. The data also show that systemic exposure of dasatinib (the driving force for brain distribution) remained relatively unchanged in the KO mice.

Differential Distribution and Efficacy of Dasatinib in the Brain

We examined the ability of dasatinib to traverse the BBB in the different brain regions of tumor-bearing mice. GFP-aided tumor dissection allowed the brain to be divided into tumor core, tumor rim and normal brain, as illustrated in Figure 5A. In WT mice, mean dasatinib concentrations in the tumor core were approximately double of that measured in tumor rim and normal brain (Figure 5B). In the KO mice, brain concentrations increased by over 2-fold in the normal brain, and by up to 3-fold in the tumor rim and core relative to WT mice ($p < 0.05$).

In order to determine the impact of this difference in drug delivery on signal transduction, individual WT and KO mice were dosed with vehicle or dasatinib, and western blotting was performed on tissue samples from the tumor core, rim and normal brain to examine the efficacy of dasatinib in inhibiting phosphorylation of SRC, a direct dasatinib target, and AKT, an indirect target (30). In the vehicle treated WT and KO mice, relatively uniform levels of phosphorylated (p) SRC were detected in the tumor core, rim and normal brain tissue (Figure 5C). In contrast, p-AKT was elevated in the tumor mass relative to normal brain in all animals tested. Total SRC and AKT were relatively uniform, making these

comparisons interpretable. We also analyzed PDGFR expression and phosphorylation because it is a direct dasatinib target and presumably a driver oncogene in this animal model. Unfortunately, total PDGFR expression was extremely variable within individual animals (regionally) and between animals, making any meaningful comparison of p-PDGFR nearly impossible (data not shown). The most striking finding we observed was the difference between p-SRC in WT relative to KO mice. Dasatinib administration completely extinguished all detectable p-SRC in all three brain regions in KO mice. In marked contrast, dasatinib did not appreciably change p-SRC levels in the normal brain, minimally affected p-SRC in the rim, and noticeably (yet incompletely) inhibited p-SRC in the tumor core of WT mice. Analysis of AKT activation followed a similar trend, whereby dasatinib inhibited p-AKT levels more robustly in all three brain regions in KO mice relative to WT (Figure 5C). These data clearly establish a relationship between the brain penetration of dasatinib, as effected by BCRP/Pgp mediated efflux, and inhibition of kinase-mediated phosphorylation.

BCRP and Pgp Loss of Function Increases Survival of Glioma-bearing Mice Treated with Dasatinib

The therapeutic efficacy of dasatinib was examined by monitoring survival in WT and KO mice that were treated with a single seven-day cycle of dasatinib. The vehicle treated cohort died rapidly after initiation of the study, with the median survival time being 7 days in the WT and 9 days in the KO mice **(Figure 6)**. When treated with dasatinib, WT mice survived longer, with a median survival time of 14 days. Importantly, the most significant effect was seen in the KO mice treated with dasatinib, where survival increased dramatically to yield a median survival time of 33 days ($p=0.03$; Figure 6). These results conclusively demonstrate that dasatinib is much more effective against the tumor when drug delivery to the brain, and hence the targets, is enhanced in KO mice.

Efficacy of Dasatinib in Pgp and BCRP Expressing Human GBM Cell Lines

A subset of glioma cells from humans and murine models express BCRP and/or Pgp (31, 32). Drug efflux mediated by these transporters within the tumor cell itself can effectively create a second barrier to drug delivery, and this has been proposed as an additional mechanism of chemoresistance in GBM (reviewed in (33)). We used primary GBM xenograft lines that were established directly from human GBM resections and screened them for expression of Pgp and BCRP. Based on expression patterns of these two transporters, six xenograft lines were identified that expressed Pgp and BCRP at different levels (Figure 7A). The efficacy of dasatinib was determined in short-term explant cultures from these xenograft lines in presence and absence of the dual Pgp/BCRP inhibitor, GF120918. Generally, there was a trend for higher BCRP/Pgp expression correlating with a higher IC_{50} of dasatinib. Five out of the six cell lines tested were sensitized to dasatinib in the presence of GF120918. Notably, GF120918 had a greater effect in lines 12, 22, 26, and 46 that expressed both Pgp and BCRP, relative to lines 6 and 10, which expressed only Pgp (Figure 7A and 7B).

Discussion

Many promising molecularly-targeted agents have failed to show any clinical benefit in glioma patients. While studies investigating the failure of these agents have proposed various hypotheses, limited drug delivery is sometimes disregarded as a likely explanation. In fact, clinical reports suggest that high drug concentrations measured in resected tumor tissue are indicative of a disrupted BBB (19), leading these investigators to conclude that poor drug delivery is not a plausible mechanism for upfront treatment failure (18). The objective of this study was to highlight two fundamental realities in treatment of an infiltrative brain tumor like GBM: (i) delivery of chemotherapeutic agents into the brain can

be significantly restricted by a BBB that is not disrupted throughout the entire brain, (ii) successful therapy in GBM will require adequate drug delivery throughout the entire brain, especially to tumor cells that may efflux drugs themselves, nested in normal brain tissue with a relatively intact BBB. A detailed discussion of these concepts focused on drug delivery can be found in our recent review (33). It is equally important to understand that migratory GBM cells that invade normal brain are intrinsically more resistant to chemotherapy and radiotherapy compared to bulk tumor (reviewed in (34)). These fundamental differences in treatment sensitivity further underscore the importance of using infiltrative preclinical models to assess therapeutics, and the need to deliver higher drug levels to invasive glioma cells which may be harder to kill than bulk tumor.

A disruption in the BBB at the central core of GBM is not surprising due to the pathophysiological characteristics of the necrotic tumor that damages the surrounding capillaries. The resulting high drug concentrations in the tumor, however, are essentially irrelevant in the majority of operable patients since the tumor core is usually removed at surgery. Drug concentrations in the tissue adjacent to the tumor are the most clinically relevant because in most cases recurrence happens near the margin of surgical resection (2). An intact BBB in such areas can shield small nests of invasive tumor cells that ultimately grow to give rise to the recurrent tumor. There are several studies that show that while drug concentrations in the resected tumor can be high (even greater than plasma), concentrations are dramatically lower in brain tissue away from the tumor. This has been elegantly shown in a study by Blakeley et al, where in a human GBM patient, concentrations of methotrexate in areas centimeters away from the tumor were about an order of magnitude lower than that in the tumor (24). Pitz et al. recently reported that concentrations of several anti-cancer agents in the non-contrast enhancing regions of the brain were significantly lower than that in the contrast enhancing tumor (35). Similarly, it has been shown that concentrations of paclitaxel (36) and temozolomide (37) in the tumor periphery were lower than that in the tumor core. However, in all these prior studies, the relative importance of tight junctions versus the expression of BCRP and Pgp was not entirely clear. When using drugs that are substrates for these transporters, distinguishing this difference is critical in order to rationally develop effective drug delivery solutions. The major contribution of this study was to unequivocally link BCRP/Pgp expression to treatment failure at the level of hitting the drug target (p-SRC in this case) and overall survival. Results from pharmacokinetic studies demonstrated that the plasma concentrations of dasatinib in WT and KO mice are not significantly different, so the increased efficacy observed in KO mice is not due to changing the bioavailability of dasatinib; but due to changing brain penetration. Our results show that drug concentrations in the tumor core are not representative of whole brain concentrations. Therefore, the use of drug concentration measurements in the resected tumor tissue as a guide for clinical assessment of drug delivery to the entire brain can be misleading.

The results of this and previous studies suggest that many drugs used to treat GBM have “failed for the wrong reason” and could be revisited assuming drug delivery obstacles are overcome. The finding that increasing drug delivery to the brain translates to improved efficacy can be valuable in choosing future combinatorial drug therapy for GBM. We have shown that inhibition of Pgp and BCRP is a useful strategy to enhance brain penetration of substrate drugs (10, 11), including dasatinib (12). Elacridar (GF120918) is a well-known dual inhibitor of Pgp and BCRP that been tested extensively in mice to improve brain penetration of numerous drugs. This study shows that GF120918 can also enhance the efficacy of dasatinib in human GBM cells. There are also reports suggesting the use of drugs that are dual Pgp/BCRP substrates to competitively inhibit both transporters. These include several TKIs that have been shown to be substrates for both Pgp and BCRP. In vitro studies show that erlotinib (38), gefitinib (39), lapatinib (40) and sunitinib (41) inhibit ABC transporters, and suggest the potential use of these agents as combination therapy to improve

drug delivery to brain. It has been shown that concurrent treatment with gefitinib results in a significantly increased brain (42) and tumor exposure to topotecan in a mouse model of glioma (43). However, such combination therapies are often confounded by additive toxicities that hinder the ability to effectively saturate Pgp and BCRP, clearly indicating the need to develop and employ more potent inhibitors. On the other hand, if both BCRP and Pgp are inhibited, it may be possible to give a lower systemic dose of a drug that is an efflux substrate while still achieving enhanced brain concentrations (presumably reducing systemic toxicities). Combination therapy with a molecularly-targeted agent and a modulator of ABC transporters could be an attractive approach to counter one of the most significant challenges in glioma chemotherapy.

In summary, this study highlights the influence of restricted drug delivery across the BBB on the efficacy of dasatinib in glioma. The heterogeneous permeability of the BBB in the tumor suggests that clinical assessment of drug delivery by using the tumor core drug concentrations (in resected tissue) as a guide for the adequacy of drug delivery can be highly misleading. Inhibition of Pgp and BCRP can be explored in future clinical trials as a possible strategy to improve delivery and hence efficacy of molecularly-targeted agents.

Supplementary Material

Refer to Web version on PubMed Central for supplementary material.

Acknowledgments

We gratefully acknowledge Lajos Mates, Zsuzsanna Izsvak, Zoltan Ivics for developing and providing the SB100 transgene used in our studies.

Grant Support This work was supported in part by grants R01 CA138437 and the Children's Cancer Research Fund (W. F. Elmquist, J. R. Ohlfest), F31 NS 67937-1 (S. A. Decker), and NS69753 and CA108961 (J. N. Sarkaria).

Abbreviation List

(Pgp)	P-glycoprotein
(BCRP)	breast cancer resistance protein
(WT)	wild-type
(KO)	mice, mice deficient for Pgp and BCRP
(BBB)	blood-brain barrier
(GBM)	Glioblastoma multiforme
(TRD)	Texas Red Dextran
(mPDGFβ)	platelet derived growth factor beta
(eGFP)	enhanced green fluorescent protein

References

1. Davis FG, Kupelian V, Freels S, McCarthy B, Surawicz T. Prevalence estimates for primary brain tumors in the United States by behavior and major histology groups. Neuro Oncol. 2001; 3:152–8. [PubMed: 11465395]
2. Wen PY, Kesari S. Malignant gliomas in adults. N Engl J Med. 2008; 359:492–507. [PubMed: 18669428]

3. Grossman SA, Ye X, Piantadosi S, Desideri S, Nabors LB, Rosenfeld M, et al. Survival of patients with newly diagnosed glioblastoma treated with radiation and temozolomide in research studies in the United States. Clin Cancer Res. 2010; 16:2443–9. [PubMed: 20371685]
4. Wen PY, Brandes AA. Treatment of recurrent high-grade gliomas. Curr Opin Neurol. 2009; 22:657–64. [PubMed: 19770658]
5. Collins VP. Mechanisms of disease: genetic predictors of response to treatment in brain tumors. Nat Clin Pract Oncol. 2007; 4:362–74. [PubMed: 17534392]
6. De Witt Hamer PC. Small molecule kinase inhibitors in glioblastoma: a systematic review of clinical studies. Neuro Oncol. 2010; 12:304–16. [PubMed: 20167819]
7. Deeken JF, Loscher W. The blood-brain barrier and cancer: transporters, treatment, and Trojan horses. Clin Cancer Res. 2007; 13:1663–74. [PubMed: 17363519]
8. Pardridge WM. The blood-brain barrier: bottleneck in brain drug development. NeuroRx. 2005; 2:3–14. [PubMed: 15717053]
9. Schinkel AH, Jonker JW. Mammalian drug efflux transporters of the ATP binding cassette (ABC) family: an overview. Adv Drug Deliv Rev. 2003; 55:3–29. [PubMed: 12535572]
10. Agarwal S, Sane R, Gallardo JL, Ohlfest JR, Elmquist WF. Distribution of gefitinib to the brain is limited by P-glycoprotein (ABCB1) and breast cancer resistance protein (ABCG2)-mediated active efflux. J Pharmacol Exp Ther. 2010; 334:147–55. [PubMed: 20421331]
11. Agarwal S, Sane R, Ohlfest JR, Elmquist WF. Role of Breast Cancer Resistance Protein (ABCG2/BCRP) in the Distribution of Sorafenib to the Brain. J Pharmacol Exp Ther. 2011; 336:223–33. [PubMed: 20952483]
12. Chen Y, Agarwal S, Shaik NM, Chen C, Yang Z, Elmquist WF. P-glycoprotein and breast cancer resistance protein influence brain distribution of dasatinib. J Pharmacol Exp Ther. 2009; 330:956–63. [PubMed: 19491323]
13. Dai H, Marbach P, Lemaire M, Hayes M, Elmquist WF. Distribution of STI-571 to the brain is limited by P-glycoprotein-mediated efflux. J Pharmacol Exp Ther. 2003; 304:1085–92. [PubMed: 12604685]
14. de Vries NA, Buckle T, Zhao J, Beijnen JH, Schellens JH, van Tellingen O. Restricted brain penetration of the tyrosine kinase inhibitor erlotinib due to the drug transporters P-gp and BCRP. Invest New Drugs. 2010:1–7.
15. de Vries NA, Zhao J, Kroon E, Buckle T, Beijnen JH, van Tellingen O. P-glycoprotein and breast cancer resistance protein: two dominant transporters working together in limiting the brain penetration of topotecan. Clin Cancer Res. 2007; 13:6440–9. [PubMed: 17975156]
16. Polli JW, Olson KL, Chism JP, John-Williams LS, Yeager RL, Woodard SM, et al. An unexpected synergist role of P-glycoprotein and breast cancer resistance protein on the central nervous system penetration of the tyrosine kinase inhibitor lapatinib (N-{3-chloro-4-[(3-fluorobenzyl)oxy]phenyl}-6-[5-({[2-(methylsulfonyl)ethy l]amino}methyl)-2-furyl]-4-quinazolinamine; GW572016). Drug Metab Dispos. 2009; 37:439–42. [PubMed: 19056914]
17. Tang SC, Lagas JS, Lankheet NA, Poller B, Hillebrand MJ, Rosing H, et al. Brain accumulation of sunitinib is restricted by P-glycoprotein (ABCB1) and breast cancer resistance protein (ABCG2) and can be enhanced by oral elacridar and sunitinib coadministration. International journal of cancer. 2011; 130:223–33.
18. Hofer S, Frei K. Gefitinib concentrations in human glioblastoma tissue. J Neurooncol. 2007; 82:175–6. [PubMed: 17008949]
19. Hofer S, Frei K, Rutz HP. Gefitinib accumulation in glioblastoma tissue. Cancer Biol Ther. 2006; 5:483–4. [PubMed: 16582594]
20. Levin VA, Patlak CS, Landahl HD. Heuristic modeling of drug delivery to malignant brain tumors. J Pharmacokinet Biopharm. 1980; 8:257–96. [PubMed: 7420270]
21. Levin VA, Freeman-Dove M, Landahl HD. Permeability characteristics of brain adjacent to tumors in rats. Arch Neurol. 1975; 32:785–91. [PubMed: 1203030]
22. Berens ME, Giese A. "…those left behind." Biology and oncology of invasive glioma cells. Neoplasia. 1999; 1:208–19. [PubMed: 10935475]

23. Pitz MW, Desai A, Grossman SA, Blakeley JO. Tissue concentration of systemically administered antineoplastic agents in human brain tumors. J Neurooncol. 2011; 104:629–38. [PubMed: 21400119]
24. Blakeley JO, Olson J, Grossman SA, He X, Weingart J, Supko JG. Effect of blood brain barrier permeability in recurrent high grade gliomas on the intratumoral pharmacokinetics of methotrexate: a microdialysis study. J Neurooncol. 2009; 91:51–8. [PubMed: 18787762]
25. Lee J, Kotliarova S, Kotliarov Y, Li A, Su Q, Donin NM, et al. Tumor stem cells derived from glioblastomas cultured in bFGF and EGF more closely mirror the phenotype and genotype of primary tumors than do serum-cultured cell lines. Cancer Cell. 2006; 9:391–403. [PubMed: 16697959]
26. Wiesner SM, Decker SA, Larson JD, Ericson K, Forster C, Gallardo JL, et al. De novo induction of genetically engineered brain tumors in mice using plasmid DNA. Cancer research. 2009; 69:431–9. [PubMed: 19147555]
27. Lockman PR, Mittapalli RK, Taskar KS, Rudraraju V, Gril B, Bohn KA, et al. Heterogeneous blood-tumor barrier permeability determines drug efficacy in experimental brain metastases of breast cancer. Clin Cancer Res. 2010; 16:5664–78. [PubMed: 20829328]
28. Carlson BL, Pokorny JL, Schroeder MA, Sarkaria JN. Establishment, maintenance and in vitro and in vivo applications of primary human glioblastoma multiforme (GBM) xenograft models for translational biology studies and drug discovery. Curr Protoc Pharmacol. 2011 Chapter 14:Unit 14 6.
29. Xiong Z, Gharagozlou S, Vengco I, Chen W, Ohlfest JR. Effective CpG immunotherapy of breast carcinoma prevents but fails to eradicate established brain metastasis. Clin Cancer Res. 2008; 14:5484–93. [PubMed: 18765540]
30. Montero JC, Seoane S, Ocana A, Pandiella A. Inhibition of SRC family kinases and receptor tyrosine kinases by dasatinib: possible combinations in solid tumors. Clin Cancer Res. 2011; 17:5546–52. [PubMed: 21670084]
31. Bleau AM, Huse JT, Holland EC. The ABCG2 resistance network of glioblastoma. Cell Cycle. 2009; 8:2936–44. [PubMed: 19713741]
32. Wu A, Oh S, Wiesner SM, Ericson K, Chen L, Hall WA, et al. Persistence of CD133(+) Cells in Human and Mouse Glioma Cell Lines: Detailed Characterization of GL261 Glioma Cells with Cancer Stem Cell-Like Properties. Stem Cells Dev. 2008; 17:173–84. [PubMed: 18271701]
33. Agarwal S, Sane R, Oberoi R, Ohlfest JR, Elmquist WF. Delivery of molecularly targeted therapy to malignant glioma, a disease of the whole brain. Expert Rev Mol Med. 2011; 13:e17. [PubMed: 21676290]
34. Lefranc F, Brotchi J, Kiss R. Possible future issues in the treatment of glioblastomas: special emphasis on cell migration and the resistance of migrating glioblastoma cells to apoptosis. J Clin Oncol. 2005; 23:2411–22. [PubMed: 15800333]
35. Pitz MW, Desai A, Grossman SA, Blakeley JO. Tissue concentration of systemically administered antineoplastic agents in human brain tumors. J Neurooncol. 2011
36. Fine RL, Chen J, Balmaceda C, Bruce JN, Huang M, Desai M, et al. Randomized study of paclitaxel and tamoxifen deposition into human brain tumors: implications for the treatment of metastatic brain tumors. Clin Cancer Res. 2006; 12:5770–6. [PubMed: 17020983]
37. Rosso L, Brock CS, Gallo JM, Saleem A, Price PM, Turkheimer FE, et al. A new model for prediction of drug distribution in tumor and normal tissues: pharmacokinetics of temozolomide in glioma patients. Cancer Res. 2009; 69:120–7. [PubMed: 19117994]
38. Shi Z, Peng XX, Kim IW, Shukla S, Si QS, Robey RW, et al. Erlotinib (Tarceva, OSI-774) antagonizes ATP-binding cassette subfamily B member 1 and ATP-binding cassette subfamily G member 2-mediated drug resistance. Cancer Res. 2007; 67:11012–20. [PubMed: 18006847]
39. Leggas M, Panetta JC, Zhuang Y, Schuetz JD, Johnston B, Bai F, et al. Gefitinib modulates the function of multiple ATP-binding cassette transporters in vivo. Cancer Res. 2006; 66:4802–7. [PubMed: 16651435]
40. Dai CL, Tiwari AK, Wu CP, Su XD, Wang SR, Liu DG, et al. Lapatinib (Tykerb, GW572016) reverses multidrug resistance in cancer cells by inhibiting the activity of ATP-binding cassette subfamily B member 1 and G member 2. Cancer Res. 2008; 68:7905–14. [PubMed: 18829547]

41. Dai CL, Liang YJ, Chen LM, Zhang X, Deng WJ, Su XD, et al. Sensitization of ABCB1 overexpressing cells to chemotherapeutic agents by FG020326 via binding to ABCB1 and inhibiting its function. Biochem Pharmacol. 2009; 78:355–64. [PubMed: 19410561]

42. Zhuang Y, Fraga CH, Hubbard KE, Hagedorn N, Panetta JC, Waters CM, et al. Topotecan central nervous system penetration is altered by a tyrosine kinase inhibitor. Cancer Res. 2006; 66:11305–13. [PubMed: 17145877]

43. Carcaboso AM, Elmeliegy MA, Shen J, Juel SJ, Zhang ZM, Calabrese C, et al. Tyrosine kinase inhibitor gefitinib enhances topotecan penetration of gliomas. Cancer Res. 70:4499–508. [PubMed: 20460504]

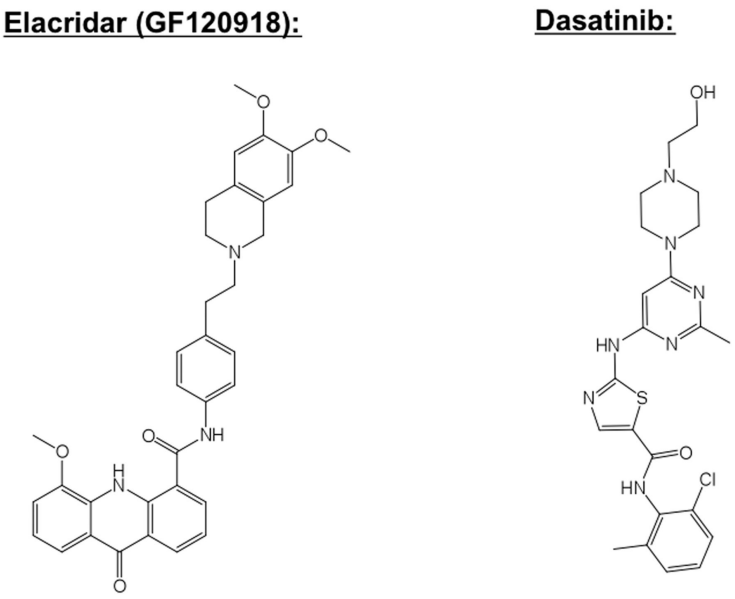

Figure 1. Chemical structures

The structure of dasatinib and GF120918 are shown.

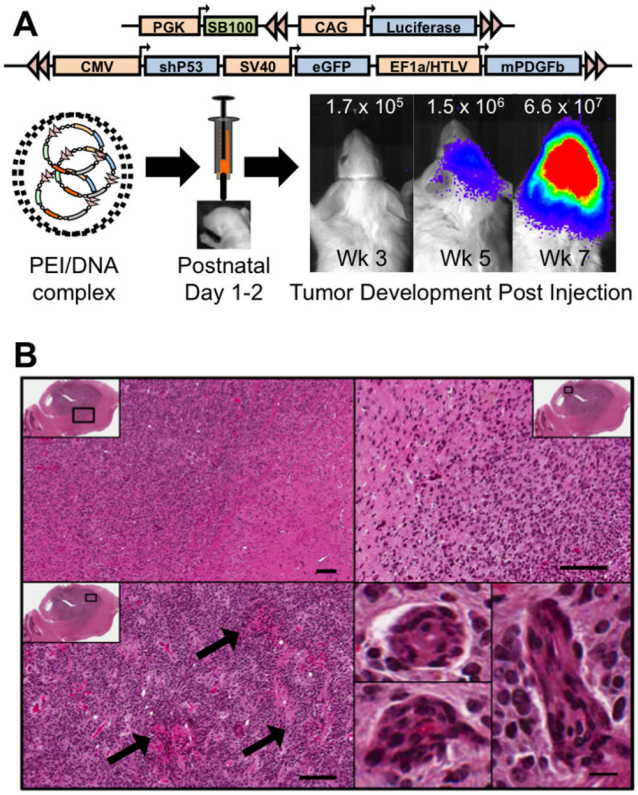

Figure 2. Oncogene-induced glioblastoma model

A, Schematic illustrating transposon vectors delivered into neonatal mice to initiate glioblastoma. Tumors were tractable by bioluminescent imaging as illustrated by a representative animal imaged longitudinally; luminescence color bar in photons/sec/cm2/Sr (min= 2×10^4, max = 1×10^6). ***B***, Representative histological features of the tumor from a moribund animal by H/E staining. Black box in low power sagittal image shows corresponding region highlighted at higher power. Top panels document infiltrative growth pattern. Arrows in lower left panel highlight areas of necrosis. Lower right panels are examples of microvascular proliferation.

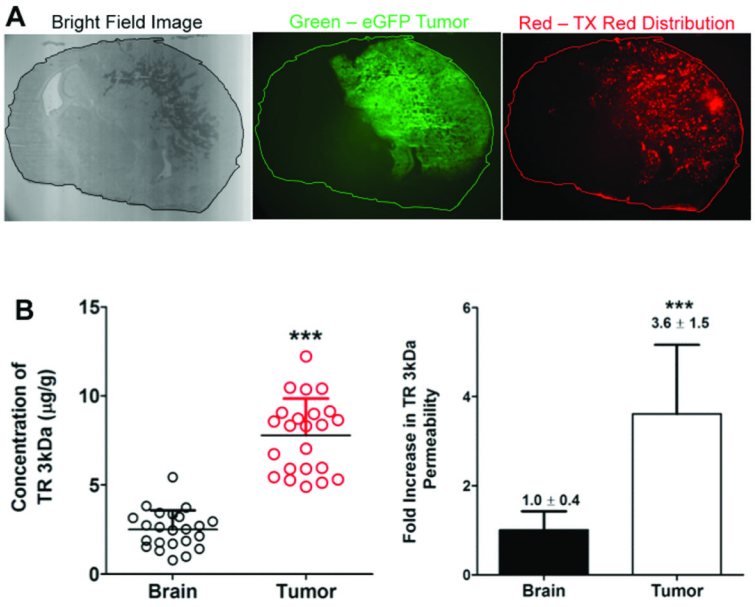

Figure 3. BBB permeability in the tumor visualized by texas red dextran

A, Four WT tumor-bearing mice were systemically injected with TRD. Representative qualitative images show higher TRD accumulation in the tumor relative to the adjacent normal brain. ***B***, The concentration of TRD is approximately 3.6 fold higher in the tumor region compared to normal brain. Each symbol represents a measurement; 5-6 measurements were made per brain in 4 total animals (***$p < 0.0001$).

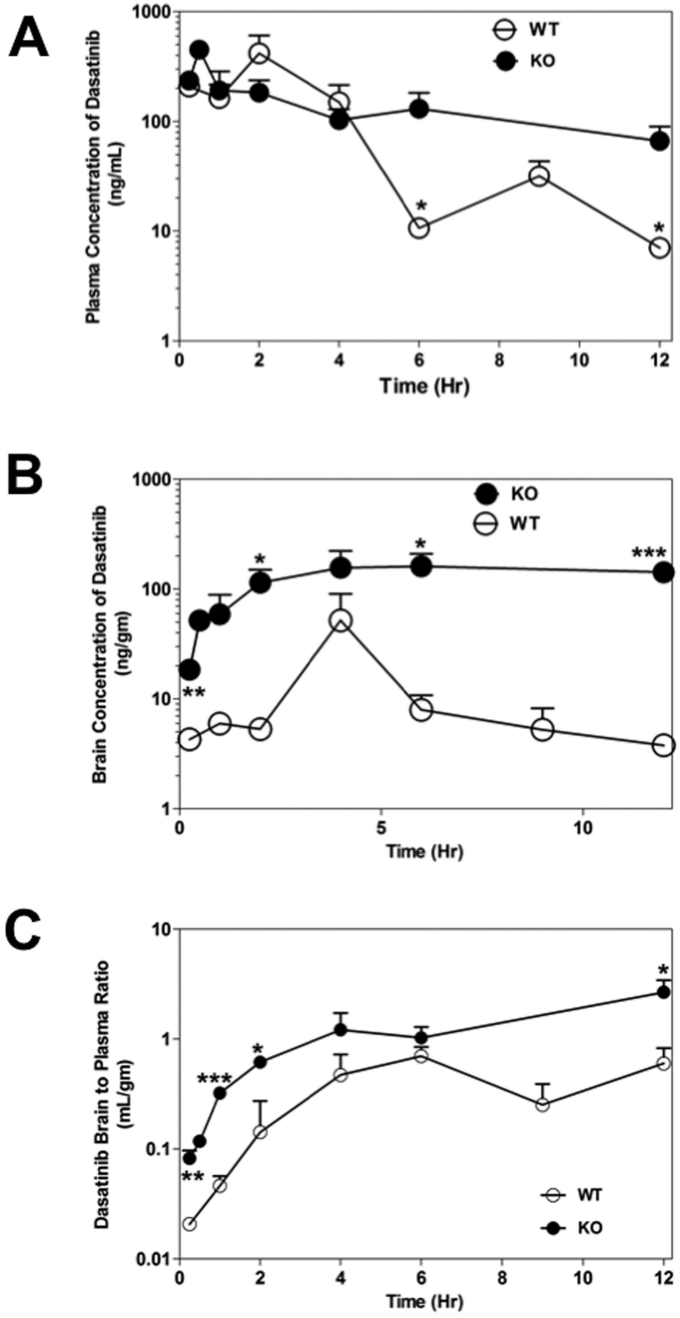

Figure 4. Comparison of dasatinib brain distribution in WT and KO mice

Panel **A** and **B** shows the plasma and brain concentrations of dasatinib, respectively, after 15 mg/kg oral dose. The brain-to-plasma ratio for dasatinib in WT and KO mice is shown in Panel **C**. Data represent mean ± SD; n=3-4 for all data points (*p<0.05, **p < 0.01, ***p ≤ 0.001).

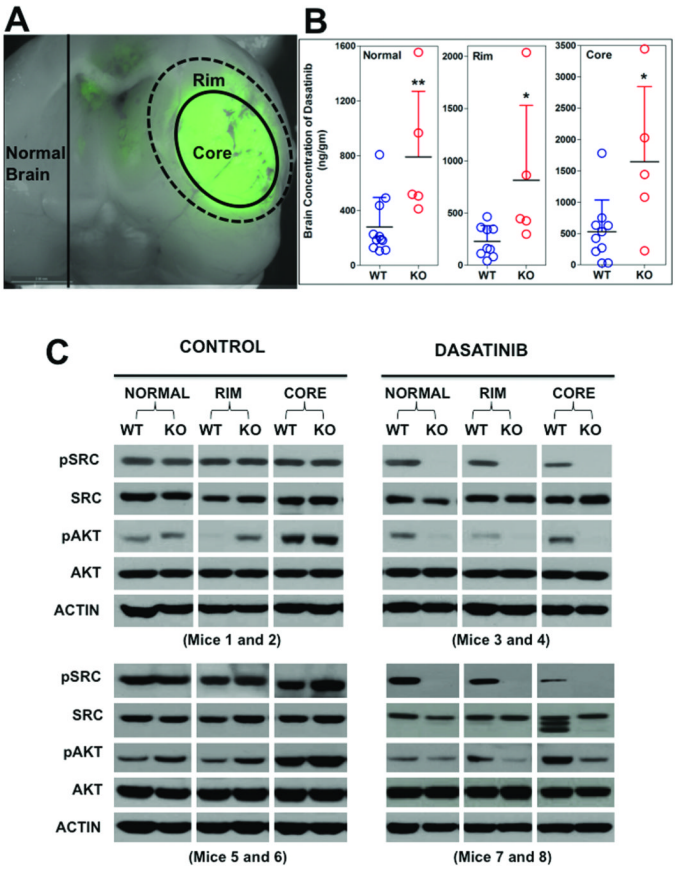

Figure 5. Regional differences in dasatinib concentration and signal transduction

A, Representative example illustrating how the brain tissue was dissected using GFP goggles. The brain was sliced in half coronally to expose the tumor expressing GFP. The center was considered the core, the tissue immediately adjacent to center was considered the rim, and the opposite hemisphere was considered normal brain. ***B***, Brain concentration of dasatinib in each region of brain tissue was quantified. Each symbol represents a measurement from an individual animal (n=9 WT, n=5 KO) (*p<0.05, **p < 0.01). ***C***, Western blot analysis of brain tissue from WT and KO mice. Representative blots from 3-4 WT and 3-4 KO total mice are shown. Each panel represents a pair of individual mice (1 WT, 1 KO) that were analyzed side-by-side on the same gel.

	N	Median (days)	P (vs. WT-Dasatinib)
KO-Dasatinib	6	33	0.03
WT-Dasatinib	8	15	NA
WT-Control	8	7	0.02
KO-Control	5	9	0.09

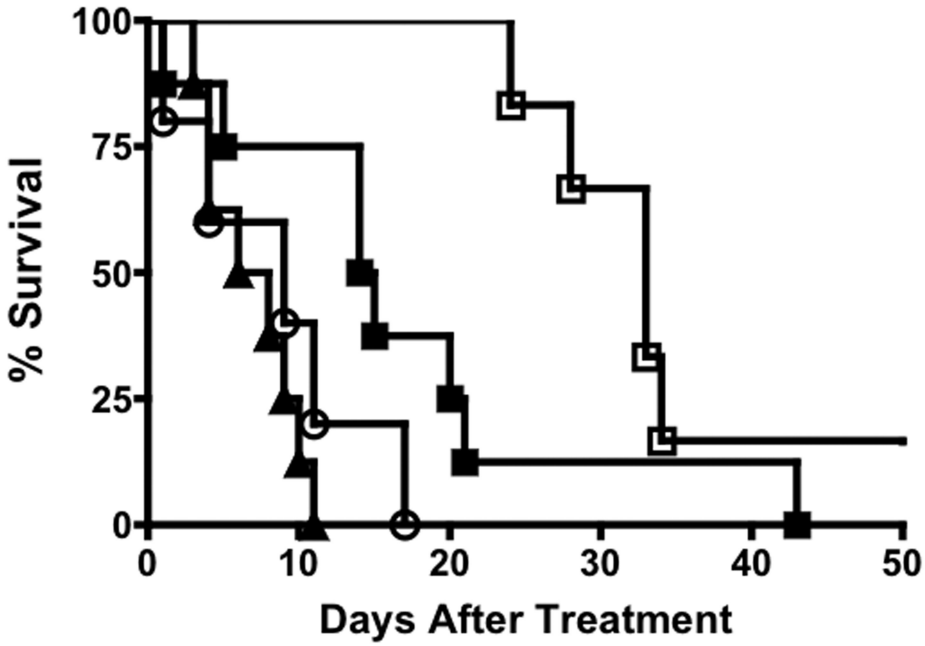

Figure 6. Enhanced efficacy of dasatinib in BCRP/Pgp deficient mice

Mice were enrolled into the indicated treatment arm as soon as tumors became apparent by bioluminescent imaging. Each group represents the cumulative survival of 5-8 individual mice that were treated at different times. The time scale indicates elapsed time from the day of enrollment. Significant differences in survival were determined by the log-rank test.

A

Cell Line	6	10	12	26	46	22
IC_{50} Dasatinib	0.80	1.6	2.1	2.5	2.5	5.6
IC_{50} Dasatinib + GF	0.94	1.2	1.2	0.78	0.65	1.2
% IC_{50} Change	+17 %	-25%	-43%	-68%	-74%	-79%

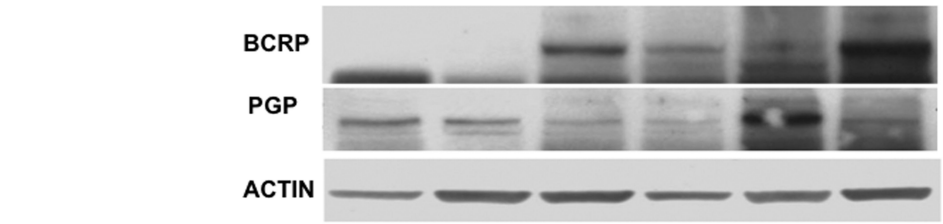

B

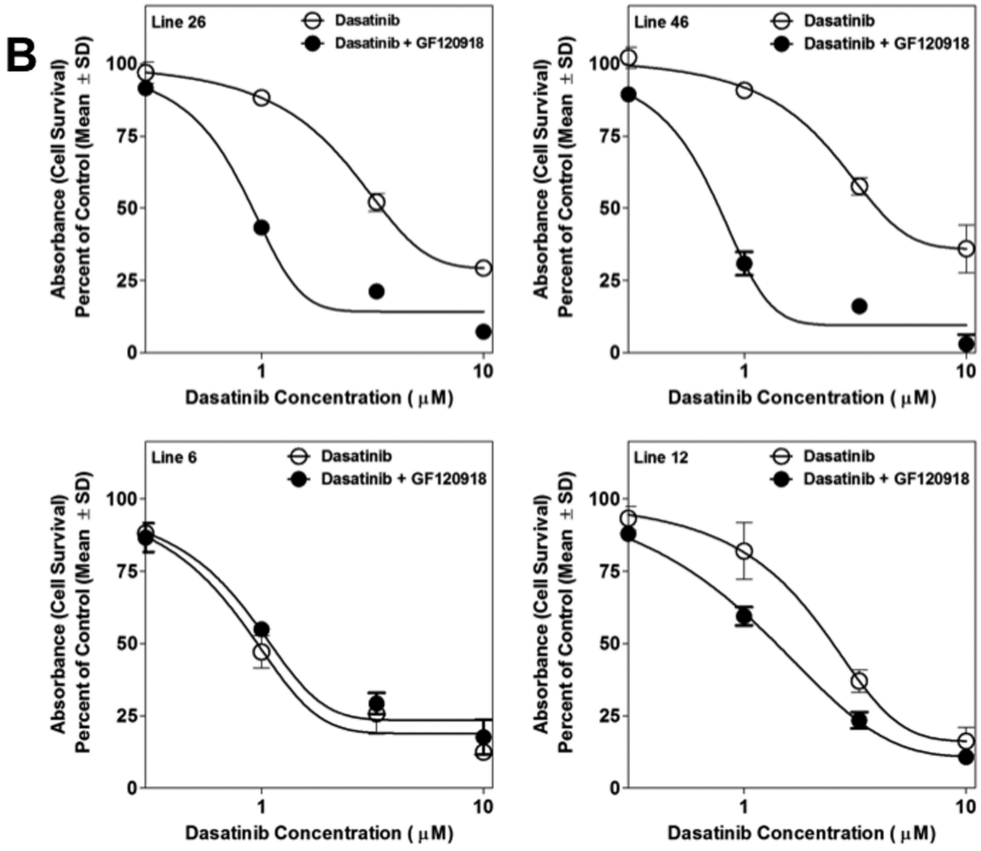

Figure 7. Inhibition of BCRP/Pgp sensitizes human glioma cells to dasatinib

A, The relative expression of BCRP and Pgp is shown by western blot in six human GBM xenograft lines. The IC_{50} values in the presence of absence of GF120918 is shown directly above the corresponding cell lines in the western blot. ***B***, Representative cell survival curves of four of the cell lines shown in A.